# Synthesis, structure and magnetic properties of the pillared perovskites La$_5$Re$_3M$O$_{16}$($M$ = Mg, Fe, Co, Ni)

Lisheng Chi,[a] A.E.C. Green,[a] R. Hammond,[b] C.R. Wiebe,[c] and J.E. Greedan[a],*

[a] Department of Chemistry, Brockhouse Institute for Materials Research, McMaster University, Hamilton, Ontario L8S 4M1, Canada
[b] Neutron Program for Materials Research, NRC, McMaster University, Canada
[c] Department of Physics and Brockhouse, Institute for Materials Research, McMaster University, Hamilton, Ontario L8S 4M1, Canada

## Abstract

Four new compounds La$_5$Re$_3$MgO$_{16}$ La$_5$Re$_3$FeO$_{16}$ La$_5$Re$_3$CoO$_{16}$ La$_5$Re$_3$NiO$_{16}$ have been prepared by solid-state reaction and characterized by X-ray and neutron powder diffraction and SQUID magnetometry. Rietveld refinement revealed that the four compounds are isostructural with La$_5$Re$_3$MnO$_{16}$ and crystallize in space group $C\bar{1}$ with cell parameters $a$ = 7.9370(3), 7.9553(5), 7.9694(7), and 7.9383(4) Å; $b$ = 7.9998(3), 7.9960(6), 8.0071(8), and 7.9983(5) Å; $c$ = 10.1729(4), 10.1895(7), 10.182(1), and 10.1732(6) Å; $\alpha$ = 90.190(3)°, 90.270(3)°, 90.248(4)°, 90.287(3)°; $\beta$ = 94.886(2)°, 95.082(3)°, 94.980(4)°, 94.864(3)°; $\gamma$ = 89.971(4)°, 90.001(5)°, 89.983(6)°, 89.968(4)° for Mg, Fe, Co, and Ni, respectively. The structures are related to a layered perovskite. The layers of corner-sharing octahedra Re$^{5+}M^{2+}$O$_6$ ($M^{2+}$ = Mg, Fe, Co, Ni) are pillared by diamagnetic edge-sharing octahedra dimers, Re$_2$O$_{10}$, involving a Re = Re double bond. Three crystallographically independent lanthanum atoms occupy the three-dimensional interstices. All compounds obey the Curie–Weiss law at sufficiently high temperatures with Curie constants or effective magnetic moments near the expected values for the combination of Re$^{5+}$ ($S$ = 1) and $M^{2+}$ ($S$ = 0, 2, 3/2, 1 for Mg, Fe, Co, and Ni, respectively). Weiss constants, $\theta_C$, are negative (−575, −84, −71, and −217 K for Mg, Fe, Co, and Ni, respectively) indicating the predominance of antiferromagnetic exchange coupling. The phases for $M$ = Fe, Co and Ni show long-range order at 155, 33, 36 and 14 K, respectively. Neutron diffraction discloses a magnetic structure for the Fe series member consisting of ferrimagnetic perovskite layers coupled antiparallel along the stacking $c$-axis, direction which is consistent with the magnetic structure found recently for La$_5$Re$_3$MnO$_{16}$.

## 1. Introduction

In recent decades, layered perovskite-type transition metal oxides have attracted great attention in the fields of chemistry, physics and materials. Obvious examples are the cuprate superconductors which are structurally related to ABO$_3$ perovskites and the alkali earth-doped rare-earth manganate perovskites La$_{1-X}$A$_X$MnO$_3$ ($X$ = Sr, Ca, Ba) [1] which exhibit fascinating physical phenomena such as colossal magnetoresistance, metal–insulator transitions, charge ordering and orbital ordering. Another perovskite-type compound Sr$_2$FeMoO$_6$ [2] is a so-called half-metallic ferromagnet with a transition temperature far above room temperature.

Compared to $3d$ transition metal oxides, their $4d$ and $5d$ counterparts have been much less explored. The $4d$ and $5d$ transition metal oxides exhibit different crystal structures and crystal chemistry from $3d$ oxides owing to the more extended nature of the $4d$ and $5d$ orbitals, the predominance of higher oxidation states and a tendency to form metal–metal bonds, among others. Recently, a new perovskite-related structure type has been reported independently by two groups. [3,4] The composition is $Ln_5M_3M'$O$_{16}$ with $Ln$ = a lanthanide and $M$ and $M'$ = Mo or $M$ = Re and $M'$ = Mn. The structure features perovskite-like corner-sharing octahedral layers, Mo$_2$O$_6$ or MnReO$_6$, which are pillared by Mo$_2$O$_{10}$ or Re$_2$O$_{10}$ dimeric units involving metal–metal double bonds. Very recent results for the Mo-based series indicate that divalent transition metal ions can partially occupy one of the intralayer Mo sites [5]. The $Ln^{3+}$ ions occupy interstitial sites. The interlayer

*Corresponding author.
E-mail address: greedan@mcmail.cis.mcmaster.ca (J.E. Greedan).

separation is $\sim 10$ Å but, surprisingly, both series of compounds show evidence for long-range magnetic order at rather high temperatures, 160–180 K [4,6,7]. In this work, the crystal chemistry and structure/property relationships of related phases in which various divalent metal ions $M^{2+} =$ Mg, Fe, Co, Ni are substituted for $Mn^{2+}$ in $La_5Re_3MnO_{16}$ are explored. The details of their synthesis, structure, magnetism and in the case of the Fe material, the magnetic structure are reported.

## 2. Experimental

### 2.1. Synthesis

The starting reagents $La_2O_3$(99.9%, Aldrich), CoO(99.5%, CERAC), NiO(99.995%, CERAC), MgO(99.95%, Alfa Aesar), $ReO_3$ (rhenium alloys) and Re (rhenium alloys) were used to synthesize polycrystalline title compounds $La_5Re_3MO_{16}$ ($M =$ Mg, Fe, Co, Ni) according to the reaction

$$5La_2O_3 + 5ReO_3 + Re + MO$$
$$\rightarrow 2La_5Re_3MO_{16}(M = \text{Mg, Fe, Co, Ni}).$$
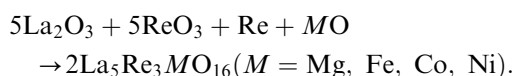
$La_2O_3$ was dried at 800°C for overnight before use. FeO was prepared by firing $Fe_2O_3$ (Fisher) and Fe at 900°C for 12 h. Because of the well-known nonstoichiometry for FeO [8], it was necessary to add excess Fe to obtain a stoichiometric product for $La_5Re_3FeO_{16}$ reaction.

Stoichiometric amounts $La_2O_3$, $ReO_3$, Re and $MO$ ($M =$ Mg, Fe, Co, Ni) were accurately weighed, ground together, loaded in a platinum crucible, sealed into a quartz tube under high vaccum ($> 10^{-5}$ mmHg), and reacted at 1050°C for 48 h.

### 2.2. X-ray and neutron diffraction

X-ray powder diffraction data were obtained using a Guinier-Hagg camera with $CuK\alpha_1$ radiation ($\lambda = 1.54056$ Å) and high-purity silicon powder as an internal standard. As well, diffraction data were collected on a Bruker D8 diffractometer using $CuK\alpha$ radiation in the $2\theta$ range from 10° to 80°. A $2\theta$ step size of 0.025° and a step time of 12 s were used. Neutron diffraction data collections were performed on the C2 diffractometer operated by the Neutron Program for Materials Research at the AECL Chalk River Laboratories. The angular ranges $10° \leqslant 2\theta \leqslant 116.9°$ at room temperature (298 K) and $3° \leqslant 2\theta \leqslant 81.9°$ at low temperature (below 160 K) were scanned with the same step interval of 0.1°. Two different wavelengths, 1.328 and 2.372 Å, were used, respectively, to collect room temperature and low temperature data for crystal structure refinement (short wavelength) and magnetic structure determination (long wavelength).

### 2.3. Magnetic properties

Magnetic susceptibility data were collected using a Quantum Design MPMS SQUID magnetometer. Zero-field cooled and field cooled (ZFC/FC ) and isothermal magnetization measurements were performed on samples in gelatin capsule containers. An oven insert was used to collect high-temperature(300–600 K) susceptibility data.

## 3. Results and discussion

### 3.1. Structural characterization

As no single crystals were available, structure analysis was carried out with powder diffraction data, both X ray and neutron. The Guinier powder patterns for $M =$ Mg, Fe, Co and Ni were observed to be similar to that for $La_5Re_3MnO_{16}$ and all reflections could be indexed on a C-centered triclinic cell. Consequently, the refinements of the room temperature powder diffraction data were carried out with the $La_5Re_3MnO_{16}$ model in space group $C\bar{1}$ [4]. The FULLPROF program [9] in the WIN-PLOTR format was used with both X-ray and neutron data. Not surprisingly, analysis of the neutron data yielded superior results with respect to the metal–oxygen distances and geometry and these are presented here. The unit-cell constants and agreement indices are shown in Table 1 with the final atomic coordinates displayed in Tables 2–5. Selected bond lengths and angles are listed in Table 6. The observed, calculated and difference diffraction profiles are plotted in Figs. 1a–d.

As can be seen from examination of Tables 2–5, it was not always possible, even with the neutron data to refine, individually, the displacement parameters for all of the atoms to positive, definite values. In fact this was accomplished only for the $M =$ Fe case. In the case of $La_5Re_3CoO_{16}$ the displacement factors were fixed to the values of $La_5Re_3MnO_{16}$.

From these results it is clear that all four compounds $La_5Re_3MO_{16}$ ($M =$ Mg, Fe, Co, Ni) are isostructural with $La_5Re_3MnO_{16}$, which has a pillared perovskite structure as illustrated for $La_5Re_3FeO_{16}$ in Fig. 2. The upper part shows the perovskite plane consisting of iron and rhenium ions which are octahedrally coordinated. Intralayer cation order is evident. The iron and rhenium(2) octahedra are interlinked through O7 along the $b$ direction and O8 along the $a$ direction. As determined for the $M =$ Mn material, the formal oxidation states of Re and $M$ are $+5$ and $+2$, respectively[4]. The unit-cell volume scales roughly with the $M^{2+}$ radius as seen in Fig. 3.

The perovskite layers are stacked along $c$ direction and separated or pillared by dimeric $Re(1)_2O_{10}$ units formed by $Re(1)O_6$ octahedra sharing a common edge

Table 1
The final refinement results for $La_5Re_3MO_{16}$ ($M = $ Mg, Fe, Co, Ni)

| Compound | $La_5Re_3MgO_{16}$ | $La_5Re_3FeO_{16}$ | $La_5Re_3CoO_{16}$ | $La_5Re_3NiO_{16}$ |
|---|---|---|---|---|
| Data source | Neutron | Neutron | Neutron | Neutron |
| Space group | $C\bar{1}$ | $C\bar{1}$ | $C\bar{1}$ | $C\bar{1}$ |
| Cell parameters | $a = 7.9359(5)$ Å | $a = 7.9553(5)$ Å | $a = 7.9694(7)$ Å | $a = 7.9383(4)$ Å |
| | $b = 7.9963(5)$ Å | $b = 7.9960(6)$ Å | $b = 8.0071(8)$ Å | $b = 7.9983(5)$ Å |
| | $c = 10.1683(7)$ Å | $c = 10.1895(7)$ Å | $c = 10.182(1)$ Å | $c = 10.1732(6)$ Å |
| | $\alpha = 90.196(4)°$ | $\alpha = 90.270(3)°$ | $\alpha = 90.248(4)°$ | $\alpha = 90.287(3)°$ |
| | $\beta = 94.878(3)°$ | $\beta = 95.082(3)°$ | $\beta = 94.980(4)°$ | $\beta = 94.864(3)°$ |
| | $\gamma = 89.966(6)°$ | $\gamma = 90.001(5)°$ | $\gamma = 89.983(6)°$ | $\gamma = 89.968(4)°$ |
| | $V = 642.92(7)$ Å$^3$ | $V = 645.61(8)$ Å$^3$ | $V = 647.3(1)$ Å$^3$ | $V = 643.60(6)$ Å$^3$ |
| Agreement factors | $R_p = 2.92$ | $R_p = 3.77$ | $R_p = 2.72$ | $R_p = 3.22$ |
| | $R_{wp} = 3.93$ | $R_{wp} = 4.92$ | $R_{wp} = 3.55$ | $R_{wp} = 4.25$ |
| | $\chi^2 = 3.20$ | $\chi^2 = 1.24$ | $\chi^2 = 1.21$ | $\chi^2 = 2.95$ |
| | $R_B = 3.59$ | $R_B = 5.76$ | $R_B = 5.71$ | $R_B = 4.37$ |

Table 2
Atomic coordinates and displacement factors, $B$ (Å$^2$), for $La_5Re_3MgO_{16}$

| Name | $x$ | $y$ | $z$ | $B$ (Å$^2$) |
|---|---|---|---|---|
| La1 | 0.228(1) | 0.746(1) | 0.8027(7) | 0.1(1) |
| La2 | 0.230(1) | 0.263(1) | 0.798(8) | 0.5(1) |
| La3 | 0.50000 | 0.50000 | 0.50000 | 0.5(1) |
| Re1 | 0.0566(6) | 0.499(1) | 0.3936(4) | 0.1 |
| Re2 | 0.00000 | 0.00000 | 0.00000 | 0.1 |
| Mg | 0.00000 | 0.50000 | 0.00000 | 0.4(2) |
| O1 | 0.1925(9) | 0.506(2) | 0.5653(7) | 0.4(1) |
| O2 | 0.2793(9) | 0.499(2) | 0.3230(7) | 0.5(1) |
| O3 | −0.0393(8) | 0.502(2) | 0.1977(7) | 0.2(1) |
| O4 | 0.0720(9) | 0.006(2) | 0.1845(8) | 0.4(1) |
| O5 | 0.037(2) | 0.734(1) | 0.365(1) | 0.2(2) |
| O6 | 0.039(1) | 0.264(1) | 0.369(1) | 0.7(2) |
| O7 | −0.048(1) | 0.247(1) | −0.001(1) | 0.9(2) |
| O8 | 0.237(1) | 0.0404(9) | −0.0346(8) | 0.5(2) |

Table 4
Atomic coordinates for $La_5Re_3CoO_{16}$

| Name | $x$ | $y$ | $z$ |
|---|---|---|---|
| La1 | 0.227(1) | 0.746(1) | 0.8024(9) |
| La2 | 0.233(1) | 0.264(1) | 0.800(1) |
| La3 | 0.50000 | 0.50000 | 0.50000 |
| Re1 | 0.0565(8) | 0.499(1) | 0.3956(6) |
| Re2 | 0.00000 | 0.00000 | 0.00000 |
| Co | 0.00000 | 0.50000 | 0.00000 |
| O1 | 0.187(1) | 0.508(2) | 0.5662(9) |
| O2 | 0.280(1) | 0.499(2) | 0.323(1) |
| O3 | −0.040(1) | 0.502(2) | 0.199(1) |
| O4 | 0.072(1) | 0.010(2) | 0.184(1) |
| O5 | 0.036(2) | 0.735(2) | 0.367(1) |
| O6 | 0.041(2) | 0.266(2) | 0.367(1) |
| O7 | −0.055(1) | 0.243(1) | −0.003(1) |
| O8 | 0.236(1) | 0.048(1) | −0.034(1) |

Table 3
Atomic coordinates and displacement factors, $B$ (Å$^2$), for $La_5Re_3FeO_{16}$

| Name | $x$ | $y$ | $z$ | $B$ (Å$^2$) |
|---|---|---|---|---|
| La1 | 0.232(1) | 0.745(1) | 0.8007(9) | 0.1(1) |
| La2 | 0.231(1) | 0.264(1) | 0.798(1) | 0.7(2) |
| La3 | 0.50000 | 0.50000 | 0.50000 | 0.4(2) |
| Re1 | 0.0567(8) | 0.499(1) | 0.393(5) | 0.04(8) |
| Re2 | 0.00000 | 0.00000 | 0.00000 | 0.04(8) |
| Fe | 0.00000 | 0.50000 | 0.00000 | 0.7(2) |
| O1 | 0.190(1) | 0.504(2) | 0.5679(9) | 0.6(2) |
| O2 | 0.277(1) | 0.498(2) | 0.3239(9) | 0.5(2) |
| O3 | −0.041(1) | 0.502(2) | 0.200(1) | 0.4(2) |
| O4 | 0.071(1) | −0.001(2) | 0.182(1) | 0.9(2) |
| O5 | 0.036(2) | 0.738(1) | 0.365(1) | 0.3(2) |
| O6 | 0.037(2) | 0.268(2) | 0.368(1) | 0.8(2) |
| O7 | −0.049(1) | 0.243(2) | 0.001(1) | 1.0(2) |
| O8 | 0.238(1) | 0.043(1) | −0.034(1) | 0.7(2) |

Table 5
Atomic coordinates and displacement factors, $B$ (Å$^2$), for $La_5Re_3NiO_{16}$

| Name | $x$ | $y$ | $z$ | $B$ (Å$^2$) |
|---|---|---|---|---|
| La1 | 0.230(1) | 0.7457(9) | 0.8027(7) | 0.3(1) |
| La2 | 0.229(1) | 0.2634(8) | 0.7999(7) | 0.3(1) |
| La3 | 0.50000 | 0.50000 | 0.50000 | 0.6(1) |
| Re1 | 0.0572(5) | 0.4985(9) | 0.3936(4) | 0.2 |
| Re2 | 0.00000 | 0.00000 | 0.00000 | 0.2 |
| Ni | 0.00000 | 0.50000 | 0.00000 | 0.4(1) |
| O1 | 0.1906(9) | 0.507(1) | 0.5664(7) | 0.42(4) |
| O2 | 0.2805(8) | 0.499(1) | 0.3248(7) | 0.42(4) |
| O3 | −0.0423(8) | 0.501(1) | 0.1972(7) | 0.42(4) |
| O4 | 0.0706(8) | 0.005(1) | 0.1849(7) | 0.42(4) |
| O5 | 0.036(1) | 0.736(1) | 0.3632(9) | 0.42(4) |
| O6 | 0.040(1) | 0.265(1) | 0.3685(9) | 0.42(4) |
| O7 | −0.0505(9) | 0.246(1) | −0.0004(8) | 0.42(4) |
| O8 | 0.2366(9) | 0.0446(8) | −0.0349(7) | 0.42(4) |

Table 6
Selected bond distances and angles for $La_5Re_3MO_{16}$ ($M$ = Mg, Fe, Co, Ni)

|  | $La_5Re_3MgO_{16}$ | $La_5Re_3FeO_{16}$ | $La_5Re_3CoO_{16}$ | $La_5Re_3NiO_{16}$ |
|---|---|---|---|---|
| La(1)–O(2) | 2.41(2) | 2.42(2) | 2.41(2) | 2.42(1) |
| La(1)–O(3) | 2.48(2) | 2.50(2) | 2.49(2) | 2.47(1) |
| La(1)–O(4) | 2.56(1) | 2.50(2) | 2.60(2) | 2.55(1) |
| La(1)–O(5) | 2.64(1) | 2.61(2) | 2.67(2) | 2.62(1) |
| La(1)–O(6) | 2.63(1) | 2.63(2) | 2.63(2) | 2.64(1) |
| La(1)–O(7) | 2.57(1) | 2.59(2) | 2.55(2) | 2.56(1) |
| La(1)–O(7) | 2.55(1) | 2.57(2) | 2.52(2) | 2.54(1) |
| La(1)–O(8) | 2.87(1) | 2.91(1) | 2.93(1) | 2.90(1) |
| La(2)–O(2) | 2.42(2) | 2.43(2) | 2.44(2) | 2.45(1) |
| La(2)–O(3) | 2.42(2) | 2.41(2) | 2.42(2) | 2.40(1) |
| La(2)–O(4) | 2.42(1) | 2.46(2) | 2.38(2) | 2.44(1) |
| La(2)–O(5) | 2.58(1) | 2.57(2) | 2.62(2) | 2.57(1) |
| La(2)–O(6) | 2.61(1) | 2.62(2) | 2.59(2) | 2.62(1) |
| La(2)–O(8) | 2.46(1) | 2.47(1) | 2.42(1) | 2.43(1) |
| La(2)–O(8) | 2.86(1) | 2.85(1) | 2.80(1) | 2.83(1) |
| La(3)–O(1) | 2.583(8) × 2 | 2.617(9) × 2 | 2.64(1) × 2 | 2.603(7) × 2 |
| La(3)–O(2) | 2.402(7) × 2 | 2.407(9) × 2 | 2.40(1) × 2 | 2.385(7) × 2 |
| La(3)–O(5) | 2.55(1) × 2 | 2.53(1) × 2 | 2.54(1) × 2 | 2.553(9) × 2 |
| La(3)–O(6) | 2.53(1) × 2 | 2.57(1) × 2 | 2.57(1) × 2 | 2.549(9) × 2 |
| Re(1)–Re(1) | 2.412(6) | 2.429(8) | 2.380(8) | 2.419(6) |
| Re(1)–O(1) | 1.973(8) | 1.99(1) | 1.95(1) | 1.975(8) |
| Re(1)–O(1) | 2.056(9) | 2.04(1) | 2.02(1) | 2.043(8) |
| Re(1)–O(2) | 1.963(8) | 1.95(1) | 1.99(1) | 1.96(1) |
| Re(1)–O(3) | 2.072(9) | 2.05(1) | 2.08(1) | 2.085(8) |
| Re(1)–O(5) | 1.91(1) | 1.94(1) | 1.93(2) | 1.93(1) |
| Re(1)–O(6) | 1.89(1) | 1.87(2) | 1.89(2) | 1.88(1) |
| Re(2)–O(4) | 1.915(8) × 2 | 1.89(1) × 2 | 1.91(1) × 2 | 1.917(7) × 2 |
| Re(2)–O(7) | 2.01(1) × 2 | 1.98(1) × 2 | 2.00(1) × 2 | 2.009(8) × 2 |
| Re(2)–O(8) | 1.969(8) × 2 | 1.98(1) × 2 | 1.98(1) × 2 | 1.974(8) × 2 |
| O(4)–Re(2)–O(7) | 91.4(7) | 92.4(9) | 91.4(9) | 91.7(6) |
| O(4)–Re(2)–O(7) | 88.6(7) | 87.6(9) | 88.6(9) | 88.3(6) |
| O(4)–Re(2)–O(8) | 87.8(6) | 88.1(8) | 87.3(8) | 88.3(5) |
| O(4)–Re(2)–O(8) | 92.2(6) | 91.9(8) | 92.7(8) | 91.7(5) |
| O(7)–Re(2)–O(8) | 91.2(6) | 91.4(8) | 91.1(8) | 90.8(5) |
| O(7)–Re(2)–O(8) | 88.8(6) | 88.6(8) | 88.9(8) | 89.2(5) |
| $M$–O(3) | 2.060(7) × 2 | 2.09(1) × 2 | 2.08(1) × 2 | 2.062(7) × 2 |
| $M$–O(7) | 2.06(1) × 2 | 2.09(1) × 2 | 2.10(1) × 2 | 2.070(8) × 2 |
| $M$–O(8) | 2.111(8) × 2 | 2.11(1) × 2 | 2.14(1) × 2 | 2.121(8) × 2 |
| O(3)–$M$–O(7) | 88.1(7) | 87.2(8) | 88.1(8) | 87.3(6) |
| O(3)–$M$–O(7) | 92.0(7) | 92.8(8) | 91.9(8) | 92.7(6) |
| O(3)–$M$–O(8) | 86.1(5) | 85.6(7) | 85.7(7) | 85.6(5) |
| O(3)–$M$–O(8) | 93.9(5) | 94.4(7) | 94.3(7) | 94.4(5) |
| O(7)–$M$–O(8) | 88.2(6) | 88.7(8) | 88.4(7) | 88.7(5) |
| O(7)–$M$–O(8) | 91.8(6) | 91.3(8) | 91.6(7) | 91.3(5) |
| Re(2)–O(7)–$M$ | 158.4(4) | 157.7(5) | 155.2(5) | 157.3(3) |
| Re(2)–O(8)–$M$ | 152.9(3) | 152.6(4) | 150.8(4) | 151.5(3) |

O1–O1 as seen in the lower part of the figure. Within the $Re(1)_2O_{10}$ unit, the Re(1)–Re(1) distances are 2.380(8), 2.397(5), 2.429(8), and 2.419(6) Å for Co, Mg, Fe, and Ni, respectively. Again, Re is formally $Re^{+5}$, $5d^2$. A similar, short Re–Re distance has been found in $Nd_4Re_2O_{11}$(Re–Re:2.421(1) Å) [10] with the same formal Re oxidation state. It is reasonable to associate such a Re–Re distance with a Re≡Re double bond. In the present compounds $La_5Re_3MO_{16}$ ($M$ = Mg, Fe, Co, Ni), the four electrons in the $Re_2$ pair can be used to form a sigma and a pi bond. The existence of a Re≡Re double bond quenches the Re magnetic moment within the

dimer. A final important feature of the structure is the connectivity between the perovskite layers. As seen from Fig. 2, the dimers connect directly only the $M^{2+}$ sites and not the $Re^{5+}$ sites in the layers.

### 3.2. Magnetic measurements

#### 3.2.1. $La_5Re_3MgO_{16}$

Susceptibility data covering the range 2–600 K are shown in Fig 4. Turning first to the high temperature results seen in the inset, adherence to the Curie–Weiss law, $\chi = C/(T - \theta)$, is found only above ∼500 K with
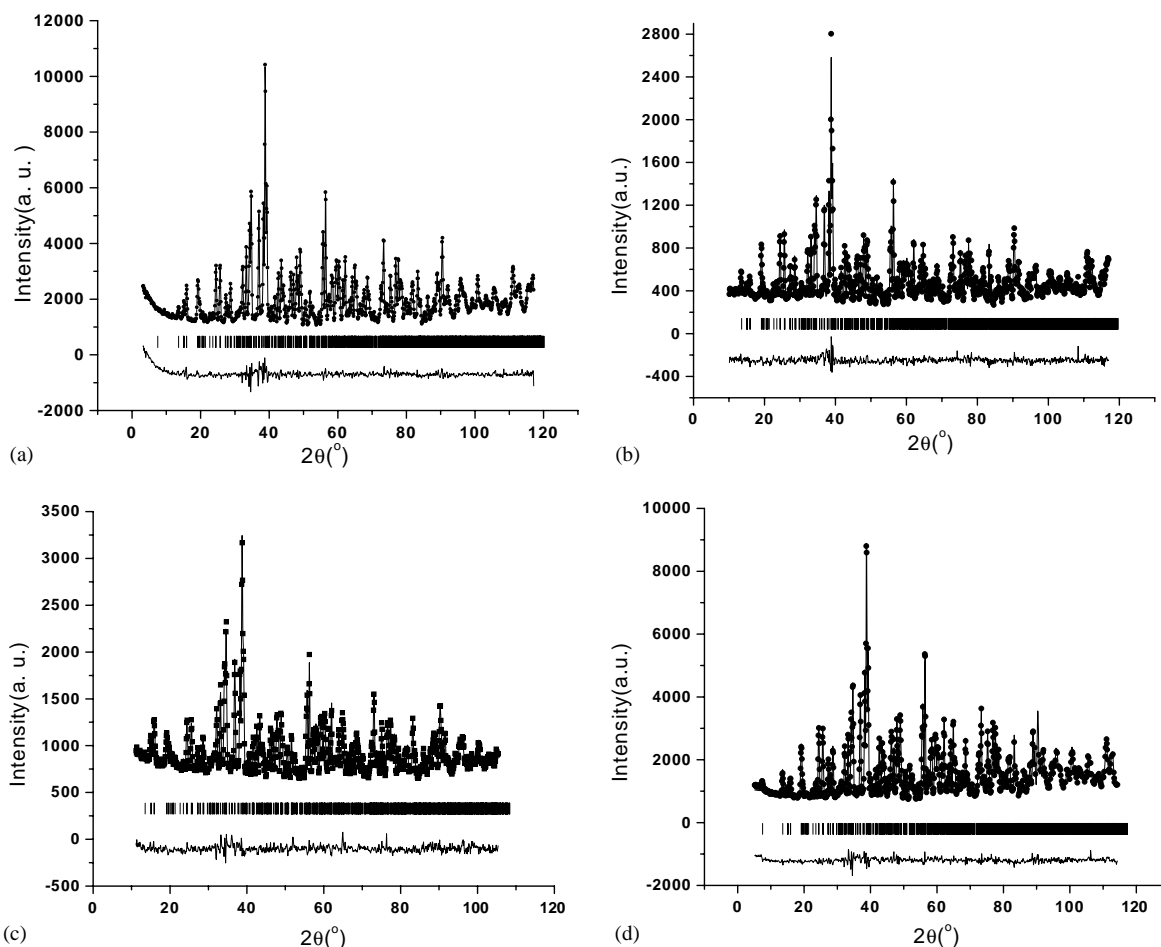
Fig. 1. (a–d) Rietveld refinements of neutron diffraction data for $La_5Re_3MO_{16}$. (a) $M = Mg$, (b) $M = Fe$, (c) $M = Co$, and (d) $M = Ni$.

fitting parameters $C = 1.00(1)$ emu K/mol and $\theta = -575(12)$ K where $C$ is Curie constant and $\theta$ is the Weiss constant. These values are consistent with a spin-only moment for $Re^{5+}$, $5d^2$, and surprisingly large, net, antiferromagnetic spin–spin correlations, given that the Re–Re interactions are mediated by O–Mg–O linkages. The regime from 2 to 350 K is dominated by two features, a strong paramagnetic response at the lowest temperatures and a very broad feature beginning below $\sim 300$ K. It is reasonable to interpret the broad feature in terms of short-range magnetic correlations. This is consistent with the layered nature of the crystal structure and the very weak interlayer connectivity between $Re^{5+}$ ions as discussed earlier. A first effort to characterize the short-range order involved an attempt to fit to the $S = 1$, two-dimensional model of lines which is appropriate for a quadratic lattice. [11]. This is shown in Fig. 5, where the low-temperature Curie–Weiss tail has been subtracted. The fit is only fair, the $g$-factor is unreasonably small at 0.77 and it was necessary to include a large TIP term of $\sim 8 \times 10^{-4}$ emu/mol. It is clear that this approach is not satisfactory.

In fact, a more careful analysis suggests that frustration may play a dominant role in the intraplanar magnetic interactions. As is seen in Fig. 6 below, a $Re^{5+}$ spin will interact with both four nearest neighbor (nn) at 5.63 Å and four next-nearest neighbor (nnn) at 7.93 Å. Both interactions involve similar superexchange pathways involving Re–O–Mg–O–Re linkages and it is not unreasonable to assume, given the very large, negative Curie–Weiss temperature, that both the nn and nnn interactions are antiferromagnetic and comparable in magnitude. In such a circumstance frustration arises, Fig. 6, as the Re spins are subject to competing exchange constraints. Such a spin system might be expected to seek an unconventional ground state such as a spin liquid or spin glass. Note from Fig. 5 that no evidence for a ZFC/FC divergence, a common signature for the spin glass or other types of statically ordered state, is seen even down to 2 K. As well, the isothermal magnetization data at 2 K (not shown) show a nearly linear dependence with no divergences out to 5.5 T. This suggests an unusual ground state and studies are currently underway to characterize this material in more detail.
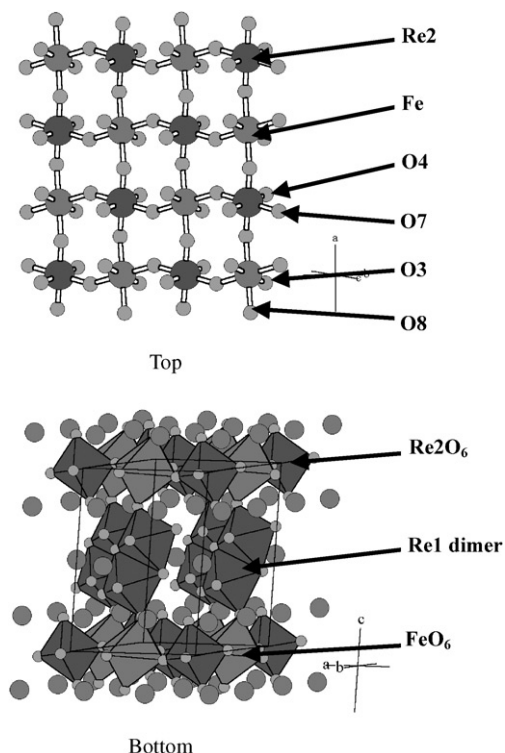
Fig. 2. Crystal structure of $La_5Re_3FeO_{16}$. Top A perovskite-like layer of corner-sharing $FeO_6$ and $ReO_6$ octahedra showing the chemical ordering of the $Fe^{2+}$ and $Re^{5+}$ ions. Bottom: A view showing the $Re_2O_{10}$ dimers which connect the perovskite-like layers. The solid spheres are the La atoms. Note that the connection pathway involves directly only the $Fe^{2+}$ ions.
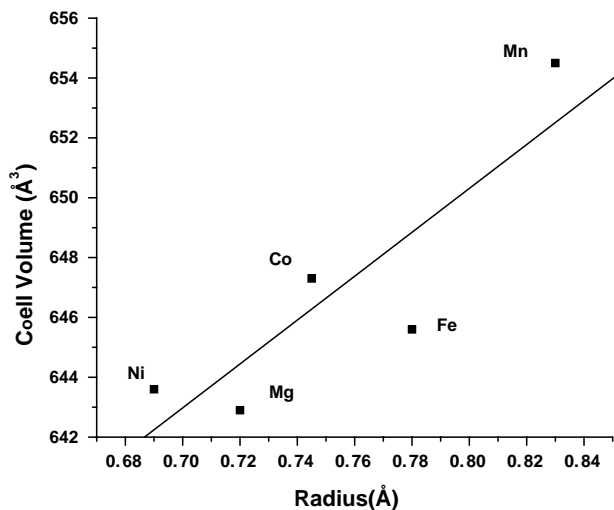


Fig. 3. Variation of unit cell volume with the $M^{2+}$ radius [16].

### 3.3. $La_5Re_3FeO_{16}$

The ZFC–FC magnetic susceptibilities of $La_5Re_3FeO_{16}$ in applied fields of 100 and 1000 Oe are plotted as a function of temperature in Fig. 7. For both applied fields, the ZFC and FC data begin to diverge below
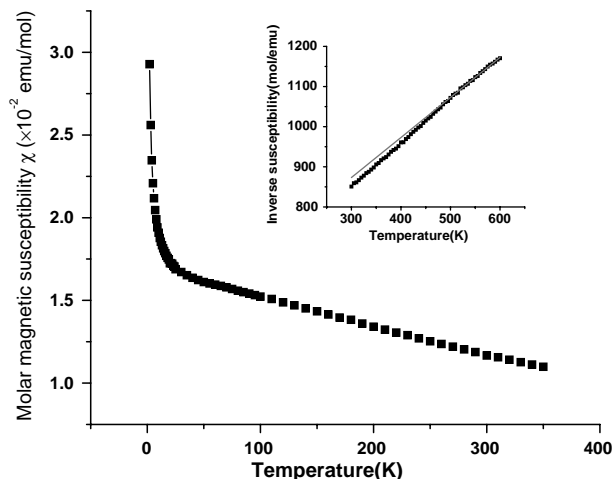


Fig. 4. Molar susceptibility data for $La_5Re_3MgO_{16}$ as a function of temperature from 2 to 600 K. The applied field was 1.0 T. The inset shows the inverse susceptibility up to 600 K and the fit to the Curie–Weiss law above 450 K. Only the ZFC curve is shown, there is no difference between the FC and ZFC curves down to 2 K.
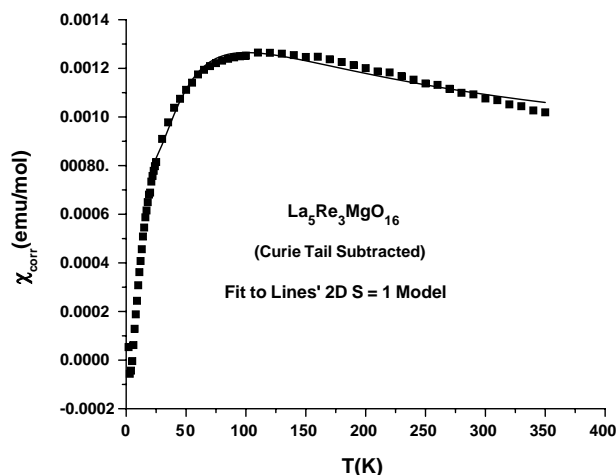


Fig. 5. An attempt to fit the susceptibility data for $La_5Re_3MgO_{16}$ (after subtraction of a low temperature Curie tail) to the Lines' function for the $S=1$ square lattice.

200 K and reach a maximum at 155 K. When the applied field is decreased to 100 Oe, the FC–ZFC divergence is more significant than that with 1000 Oe and there is a broad shoulder between 65 and 125 K. The Curie–Weiss law fit in the temperature range 520–600 K (Fig. 8) yields $\theta = -84$ K, $C = 3.60(2)$(emu/mol K), comparable to the sum of $Fe^{2+}(d^6,\ C = 3.00$(emu/mol K)) and $Re^{5+}(d^2,\ C = 1.00$ (emu/mol K)). Fig. 8 shows the isothermal magnetic field dependence of the magnetization at 5, 60, 140 and 250 K. At 5 K, the magnetization increases only gradually to $H = 4$ T followed by a weak upturn to 5.5 T. At 60 and 140 K, both magnetization curves have sharp increases at 2000 and 5000 Oe, respectively, and reach saturation magnetic moments,
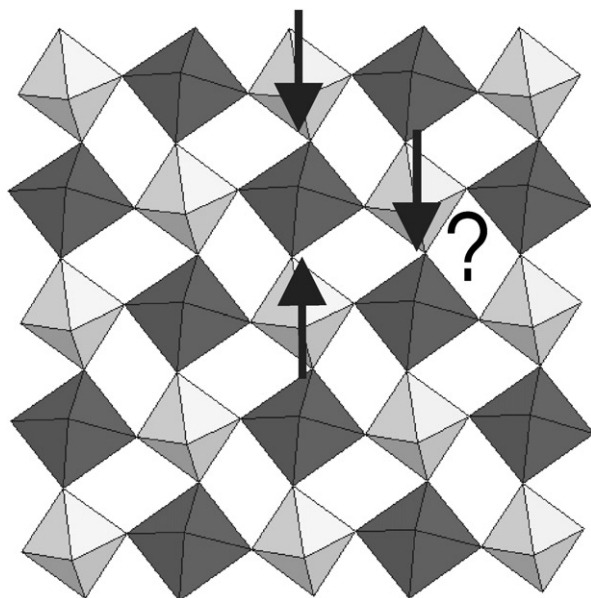
Fig. 6. Re–O–Mg–O–Re linkages between nearest neighbors and next-nearest neighbors in the perovskite layers of $La_5Re_3MgO_{16}$. The arrows represent the spin on $Re^{5+}$ ions. Note that if $J_{nn} \sim J_{nnn}$ and both are antiferromagnetic, the spins will be frustrated.
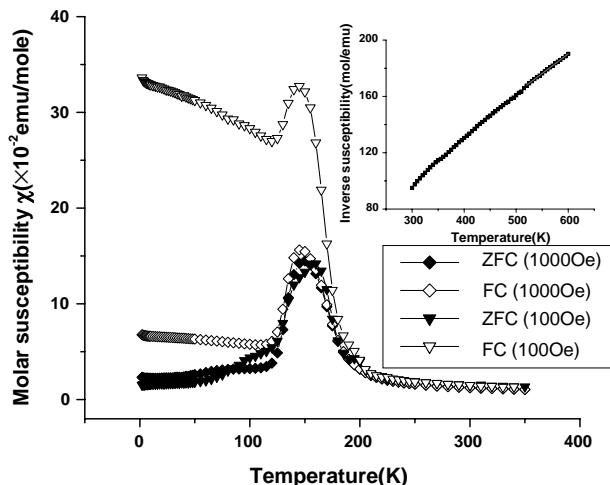


Fig. 7. ZFC and FC susceptibilities for $La_5Re_3FeO_{16}$ for applied fields of 100 and 1000 Oe. The inset shows the inverse susceptibility up to 600 K and the fitted line indicates a Curie–Weiss law above $\sim$ 500 K.



Fig. 8. Isothermal magnetization versus applied field behavior for $La_5Re_3FeO_{16}$. Note the appearance of sharp jumps at low applied fields for 140 and 60 K.

1.4 and 0.9 $\mu_B$, respectively at 4 T. At 250 K, the curve is linear which is a signature of paramagnetic behavior. Note that $\theta_C$, while still negative, is considerably smaller than that for $La_5Re_3MgO_{16}$. This suggests that the $Fe^{2+}$–$O^{2-}$–$Re^{5+}$ superexchange interaction is ferromagnetic. This is in qualitative agreement with the Goodenough–Kanamori rules for $(t_{2g}^4 \ e_g^2)$–$(t_{2g}^2)$ super-exchange [12,13]. Nonetheless, the bulk ma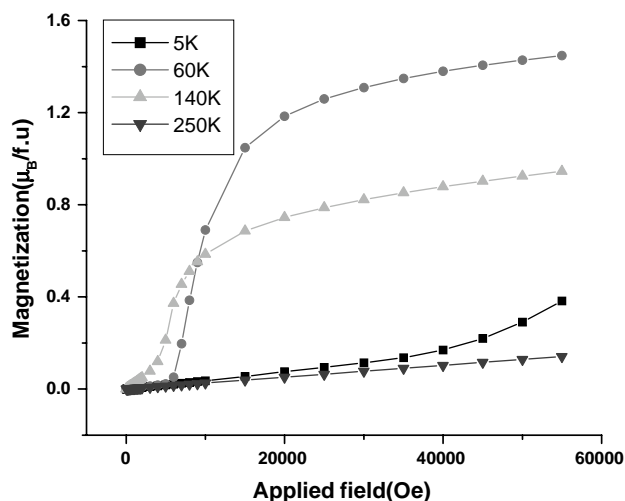gnetic data are not consistent with an overall ferromagnetic structure at least at zero applied field. For example, the $M$ vs $H$ curves show sharp transitions at moderate fields, features indicative of metamagnetic behavior, and the best saturation magnetization values are more consistent with AF $Fe^{2+}$–$Re^{5+}$ coupling. ($\mu_{sat.} \rightarrow 2\,\mu_B$) rather than $F$ coupling ($\mu_{sat.} \rightarrow 6\,\mu_B$).

Neutron diffraction is of course the most powerful technique for the characterization of magnetic order and experiments were carried out to determine the magnetic structure of $La_5Re_3FeO_{16}$. Fig. 9 shows neutron diffraction patterns in the low-angle region at selected temperatures, emphasizing the development of the major Bragg reflections. In the pattern at 13 K, the most intense of the low-angle magnetic Bragg peaks occur at $2\theta = 24.60°$, $25.44°$, $30.50°$ and $32.53°$ and can be indexed on a magnetic unit cell with $a_{mag} = a$, $b_{mag} = b$, $c_{mag} = 2c$, where $a, b, c$ are the axes of the chemical unit cell, i.e., with ordering wave vector $\mathbf{k} = (0, 0, 1/2)$. This is the same result as for $La_5Re_3MnO_{16}$ which exhibited an A-type magnetic structure consisting of ferrimagnetically coupled perovskite layers coupled antiparallel along the $c$-axis. Using the same model, the refinement of the magnetic structure of $La_5Re_3FeO_{16}$ resulted in the agreement factors with $R_p = 6.22$, $R_{wp} = 8.45$, $R_{mag} = 33.7$ $R_{exp} = 3.33$ and the structure is shown in Fig. 10 where the $Fe^{2+}$ moments of 3.0(2) $\mu_B$ are tilted from the $c$-axis by an angle of 18(1)°, while $Re^{5+}$ moments of 1.5(1) $\mu_B$ are nearly parallel to the $c$-axis, indicating that the $Re^{5+}$ and $Fe^{2+}$ moments are ferrimagnetically coupled within the layer and antiferromagnetically coupled between the layers, i.e., an A-type ordering. As shown in Fig. 11, the temperature dependence of the intensities of the magnetic reflections indicates $T_c = 155$ K which is consistent with the bulk susceptibility data of Fig. 7.
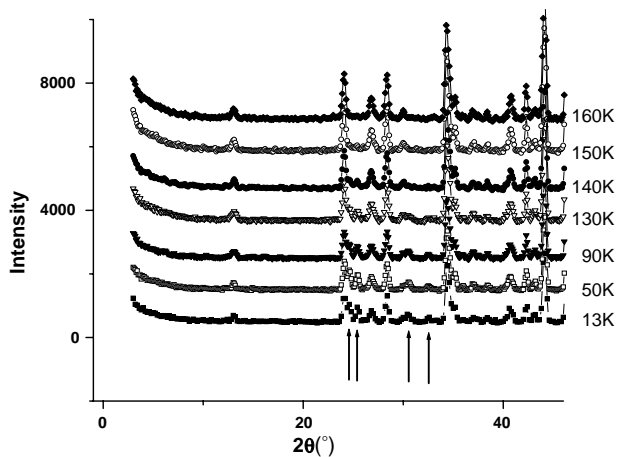
Fig. 9. Neutron diffraction patterns for $La_5Re_3FeO_{16}$ ($\lambda = 2.372$ Å) at selected temperatures showing the development of magnetic Bragg peaks (arrows).
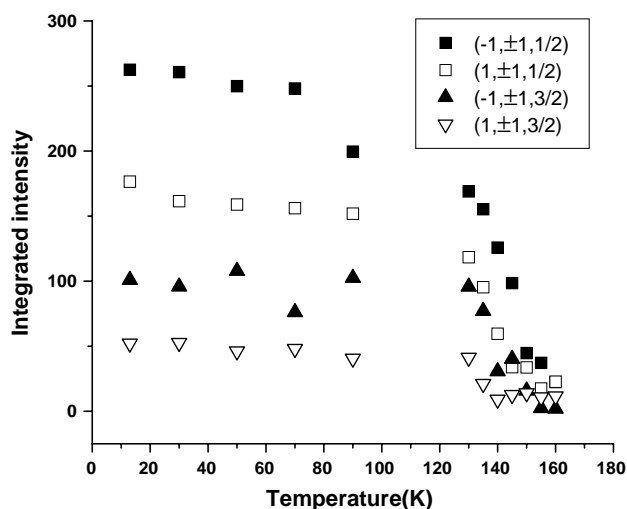


Fig. 11. The temperature dependence of the major magnetic Bragg peaks for $La_5Re_3FeO_{16}$ indicating $T_c = 155$ K.
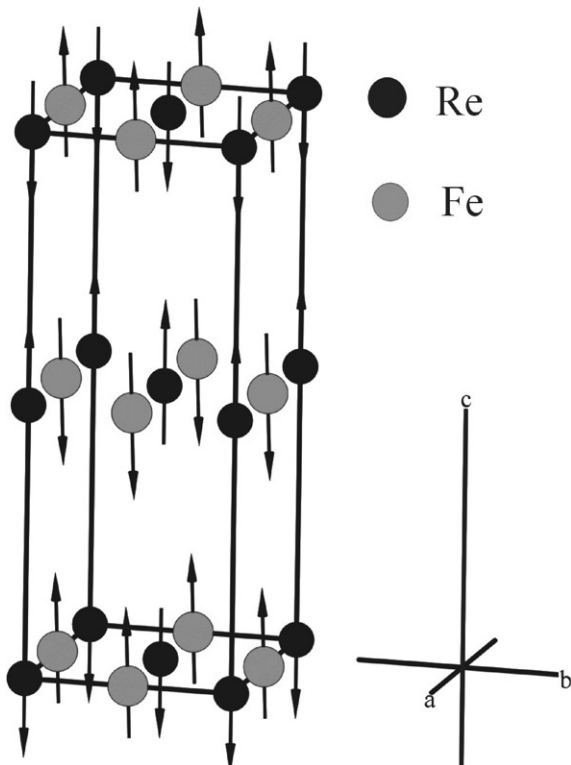


Fig. 10. The magnetic structure of $La_5Re_3FeO_{16}$ refined from neutron diffraction data at 13 K.



Fig. 12. ZFC-FC susceptibilities for $La_5Re_3CoO_{16}$ at an applied field of 1000 Oe. Note the sharp maximum at 33 K. The inset shows inverse susceptibilities up to 600 K and the fitted line shows Curie–Weiss behavior above 300 K.

## 3.4. $La_5Re_3CoO_{16}$

Fig. 12 presents the ZFC–FC magnetic susceptibilities of $La_5Re_3CoO_{16}$ as a function of temperature in an applied field of 1000 Oe. There is a sharp cusp at 33 K which can be taken as the ordering temperature, $T_c$. Curie–Weiss-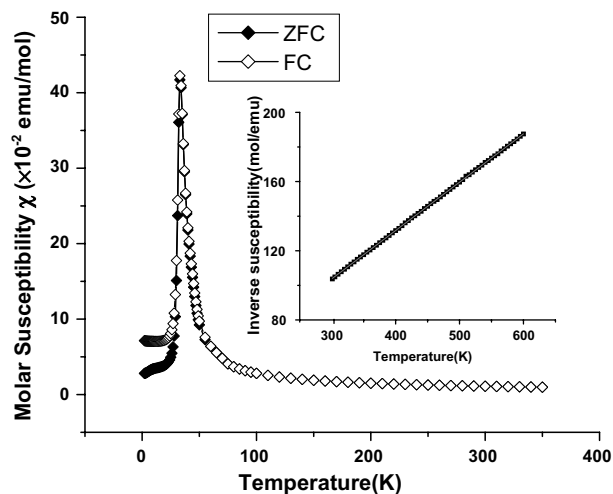like behavior sets in between 300 and 600 K and fitting yields $\theta_C = -71.2(5)$ K, and $C = 3.578(3)$ emu/mol K, which is slightly larger than that expected for $Co^{2+}(d^7)$, $C = 1.87$ emu/mol K and $Re^{5+}(d^2)$, $C = 1$ emu/mol K. This might be due to a partial orbital contribution to the magnetic moment of $Co^{2+}$. Such an orbital contribution has been used to explain the unusual magnetic moment value in $CoWO_4$ [14]. The magnetization is plotted as a function of applied field at 5, 23, 33, 60 and 100 K in Fig. 13. At 5 and 23 K, both magnetization curves have a sharp increase at 5000 Oe and approach a saturation magnetic moment of about 1.4 $\mu_B$ by 4 T. At 33 K, the magnetization curve shows an approach to saturation behavior. At 60 and 100 K, the magnetization curves indicate paramagnetic behavior.

### 3.5. La₅Re₃NiO₁₆

The ZFC–FC magnetic susceptibilities are plotted as a function of temperature in an applied field of 1000 Oe in Fig. 14. The ZFC curve shows two maxima at 36 and 14 K, respectively, while for the FC curve only the sharp cusp at 14 K is apparent but a ZFC–FC divergence occurs at 36 K. The Curie–Weiss law (inset) obtains between 450 and 600 K with $\theta_C = -217(3)$ K and

$C = 2.29(1)$ emu/mol K, comparable to the sum of $Ni^{2+}(d^8)$ $C = 1.00$ emu/mol K and $Re^{5+}(d^2)$ $C = 1.00$ emu/mol K. Fig. 15 exhibits the magnetization as a function of applied field at 5, 12, 34, and 70 K. At 5 K, the magnetization does not approach saturation even at the highest magnetic field of 5.5 T. At 12 K, the magnetization deviates only slightly from linearity in the measured range. At 34 and 70 K, the linear behavior of the magnetization indicates paramagnetic behavior.
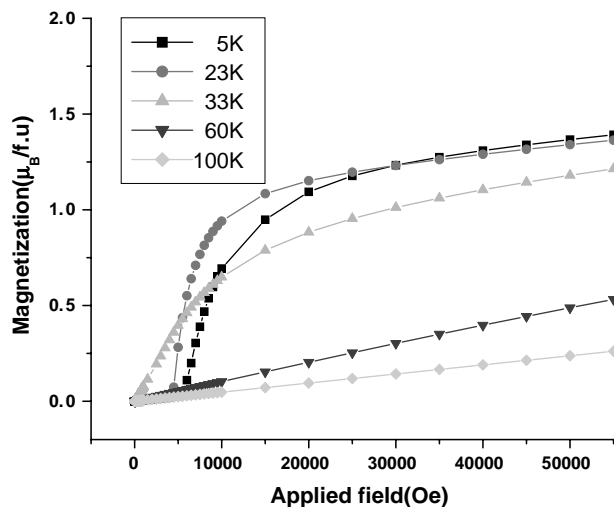


Fig. 13. Isothermal magnetization versus applied field for La₅Re₃CoO₁₆ at several temperatures. Note the appearance of sharp jumps in the magnetization for low applied fields as the temperature decreases.
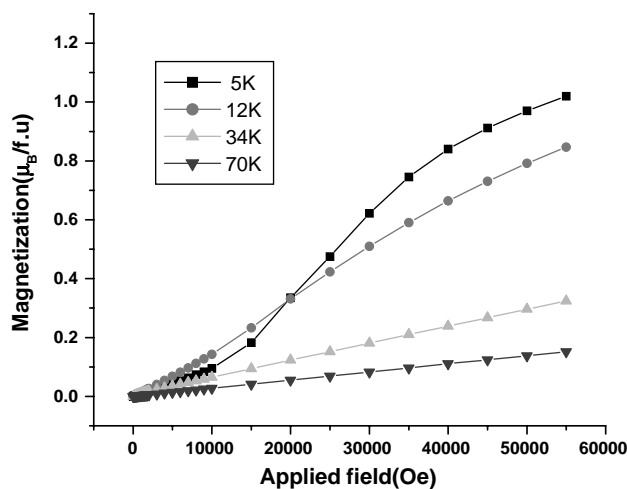


Fig. 15. Isothermal magnetization versus applied field at selected temperatures for La₅Re₃NiO₁₆. Note the appearance of relatively sharp jumps at applied fields >20 000 Oe as the temperature is decreased.



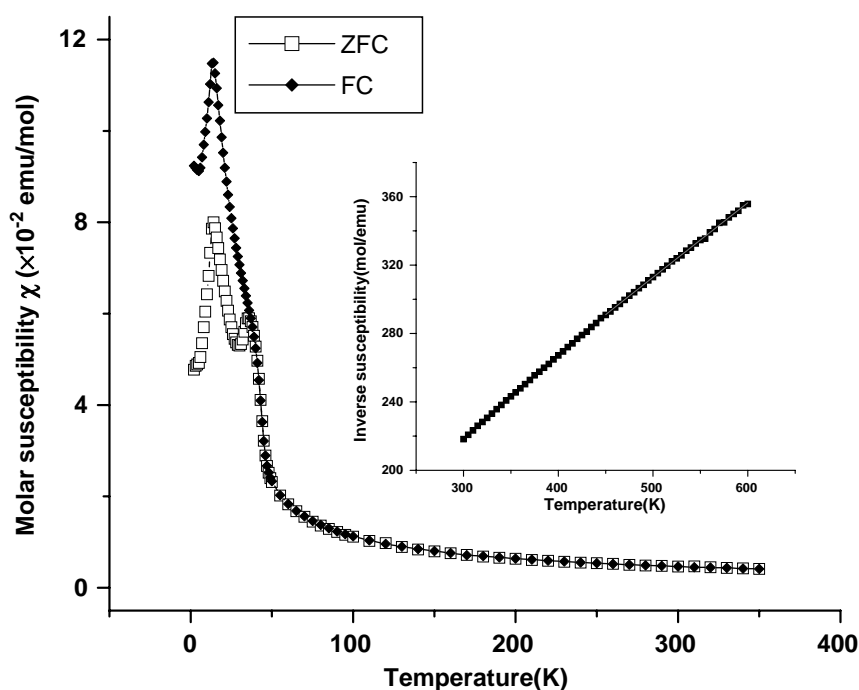Fig. 14. ZFC-FC susceptibilities for La₅Re₃NiO₁₆ at an applied field of 1000 Oe. Note the sharp maxima in the ZFC data at 36 and 14 K. The inset shows inverse susceptibilities up to 600 K. The fitted line indicates Curie–Weiss behavior above 450 K.

Table 7
Collected magnetic data for $La_5Re_3MO_{16}$.

| $M$ | $\theta_C$ (K) | $T_c$ (K) | $T_c/S^2$ (K) | $C_{obs}$ (emu K/mol) | $C_{SO}$[a] (emu K/mol) |
|---|---|---|---|---|---|
| Mn | −48(5) | 161 | 26 | 4.43(4) | 5.38 |
| Fe | −84(4) | 155 | 39 | 3.60(2) | 4.00 |
| Co | −71.2(5) | 33 | 15 | 3.578(3) | 2.87 |
| Ni | −217(3) | 36,14 | 36 | 2.29(1) | 2.00 |
| Mg | −575(12) | — | — | 1.00(1) | 1.00 |

[a] The Curie constant based on the spin-only model.

## 4. Summary and conclusions

The isostructural series, $La_5Re_3MO_{16}$ shows properties consistent with local moment magnetism at the Re(2) site and the $M$ site in the perovskite-like layers. Curie constants or effective moments obtained from Curie–Weiss fits at high temperatures are consistent with nearly spin-only values for $Re^{5+}$ and $M^{2+}$. All except $M = Mg^{2+}$ show evidence for long-range magnetic order at the temperatures given in Table 7. These temperatures are surprisingly high given that the interlayer separation is $\sim 10$ Å for all cases. There is also a strong dependence of $T_c$ on the identity of $M^{2+}$ with high values for Mn and Fe and quite low values for Co and Ni. For layered magnets a simple mean field argument suggests that $T_c \sim \xi_{intra}^2 J_{inter} S^2/k$ [15], where $\xi_{intra}$ is the intraplanar correlation length, $J_{inter}$ is the interplanar exchange coupling and $S$ is the spin. The $S^2$ dependence can be removed by dividing into $T_c$ and the result, Table 7, indicates no additional systematics with respect to $M$. One notes that $T_c/S^2$ for Co is anomalously small.

The magnetic structures for $M = Mn^{2+}$ and $Fe^{2+}$ have been solved and both show essentially the same result with ferrimagnetically coupled (but slightly canted) Re and $M$ moments within the perovskite layers which are then coupled antiferromagnetically along the layer stacking direction. Although this result is for zero field only, it provides a means to understand the metamagnetic-like transitions observed for all of the phases in the isothermal $M$ vs $H$ data. That is, the relatively weak interplanar exchange coupling is overcome by the application of modest fields of the order of 0.5 T in most cases, to give parallel interlayer coupling. The intralayer configuration remains ferrimagnetic and this is consistent with the values of the "saturation" moments for all materials which fall far below the limits for ferromagnetic coupling which are 7, 6, 5, and 4 $\mu_B$ for $M = $ Mn, Fe, Co, and Ni, respectively.

There does exist a minor paradox with respect to the observation of ferrimagnetic intraplanar coupling and the observed $\theta_C$ values. It is clear that the $Re^{5+}$–$Re^{5+}$ intraplanar exchange is very large and antiferromagnetic from the observed $\theta_C = -575$ K for $M = Mg^{2+}$, while corresponding temperatures for the other $M$ are considerably less negative. This suggests that the $Re^{5+}$–$M^{2+}$ magnetic interaction is overall ferromagnetic. This is in fact consistent with the Goodenough–Kanamori rules. $Re^{5+}$ has a $t_{2g}^2$ configuration. All of the other ions have 1/2 filled or more than 1/2 filled $t_{2g}$ levels and partially filled $e_g$ levels. The $e_g^n \rightarrow t_{2g}^2 e_g^0$ transfers from $M \rightarrow Re$ would be ferromagnetic and the overall effect should be at least weakly ferromagnetic. Nonetheless, the intralayer Re–$M$ coupling is unambiguously antiparallel (ferrimagnetic). Ultimately, perhaps, the most remarkable material of all is the $M = Mg^{2+}$ member. In spite of very large antiferromagnetic exchange already noted, this material does not appear to order down to 2 K, while deviations from the Curie–Weiss law set in near 300 K. As mentioned, the intraplanar spin–spin correlations are subject to frustration and the interplanar Re–Re superexchange pathway is extremely convoluted. This compound is under further investigation.

Finally, it is worth making some comparisons with the newly reported phases, $La_5Mo_{3+x}M_xO_{16}$, wherein the $M$ site is partially substituted by a divalent ion. [5] In this system substitution levels of $x \sim 0.75$ have been achieved using both molten salt electrolysis and solid state reaction methods. For some cases, $T_c$ can be estimated from DC and AC susceptibility data. The observed dependence of $T_c$ on $M$ is less dramatic with $T_c$ remaining near 100 K for $x = 0.75$ and $M = $ Mn, Fe and Co. These values are reduced significantly from the parent $M = $ Mo compound which shows $T_c = 200$ K.

## References

[1] M. Imada, A. Fujimori, Y. Tokura, Rev. Mod. Phys. 70 (1998) 1039.

[2] K.-I. Kobayashi, T. Kimura, H. Sawada, K. Terakura, Y. Tokura, Nature (London) 395 (1998) 677.

[3] M. Ledesert, Ph. Labbe, W.H. McCarroll, H. Leligny, B. Raveau, J. Solid State Chem. 105 (1993) 143.

[4] C.R. Wiebe, A. Gourrier, T. Langet, J.F. Britten, J.E. Greedan, J. Solid State Chem. 151 (2000) 31.

[5] K.V. Ramanujchary, S.E. Lofland, W.H. McCarroll, T.J. Emge, M. Greenblatt, M. Croft, J. Solid State Chem. 164 (2002) 60.

[6] K.V. Ramanujchary, M. Greenblatt, W.H. McCarroll, J.B. Goodenough, Mater. Res. Bull. 28 (1993) 1256.

[7] A.E.C. Green, C.R. Wiebe, J.E. Greedan, Solid State Sci. 4 (2002) 305.

[8] E.R. Jette, F. Foote, J. Chem. Phys. 1 (1933) 29.

[9] T. Roisnel, J. Rodriguez-Carvajal, Mater. Sci. Forum 378–381 (2001) 118.

[10] K.A. Wilhelmi, E. Lagervall, O. Muller, Acta Chem. Scand. 24 (1970) 3406.

[11] M.E. Lines, J. Phys. Chem. Solids 1 (1970) 101.

[12] J.B. Goodenough, Magnetism and the Chemical Bond, Wiley, New York, 1963.

[13] J. Kanamori, Phys. Chem. Solids 10 (1959) 87.

[14] J.B. Forsyth, C. Wilkinson, J. Phys.: Condens. Matter 6 (1994) 3073.

[15] L.J. de Jongh, in: L.J. deJongh (Ed.), Magnetic Properties of Layered Transition Metal Compounds, Kluwer Academic Publishers, Dordrecht, 1990, p. 19.

[16] R.D. Shannon, Acta Crystallogr. A 32 (1976) 751.